INTERNATIONAL ATOMIC ENERGY AGENCY
UNITED NATIONS EDUCATIONAL, SCIENTIFIC AND CULTURAL ORGANIZATION

INTERNATIONAL CENTRE FOR THEORETICAL PHYSICS
34100 TRIESTE (ITALY) - P.O.B. 586 - MIRAMARE - STRADA COSTIERA 11 - TELEPHONE: 2240-1
CABLE: CENTRATOM - TELEX 460392 - I

SMR/459- 17

SPRING COLLEGE IN CONDENSED MATTER
ON
'PHYSICS OF LOW-DIMENSIONAL STRUCTURES'
(23 April - 15 June 1990)

METALLIC SUPERLATTICES

Danilo PESCIA
Kernforschungsanlage Jülich GmbH
Institut für Festkorperforschung
Postfach 1913
D-5170 Jülich
Federal Republic of Germany

1. Growth-modes and structural analysis of metallic superlattices. 1.

1.1. Introduction.

Metallic superlattices can be divided into three categories:

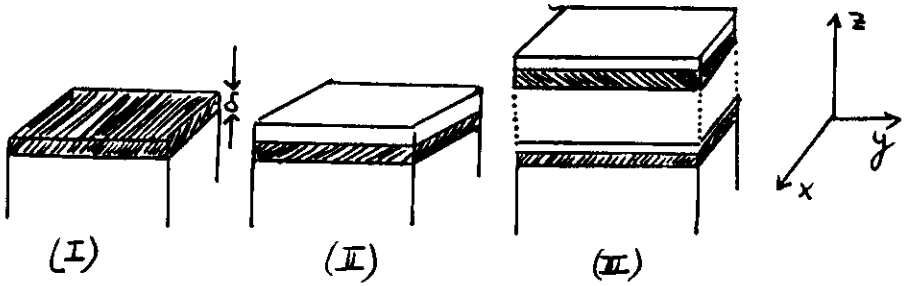

I consists of a substrate covered by a thin film of chemically different atoms (●) of thickness δ (typically 1 to 10 monolayers (ML)). II is a "sandwich" structure, where the film is covered by a coating. This structure can be repeated periodically along z to give rise to a multilayered structure III. The aim of III is to provide a sizeable amount of the ●-atoms while keeping the unique physical properties associated with the atoms ● being arranged into a nearly 2-dimensional (2d) structure – i.e. a structure extending to macroscopic lengths in the x-y plane and having a finite thickness δ along z. I is the building block of metallic superlattices, which has attracted much interest – both theoretically and experimentally – it the past 5 years. In the remainder of these lectures we will therefore focus our attention mainly on (I), although many recent experiments show that in II and III new phenomena occur, not encountered in I.

1.2. Growth of epitaxial layers.

The problem which has been solved by material science only recently – and for a small number of systems – is the manufacturing of (I) with sharp interfaces dividing the substrate-atoms from the adsorbed atoms. Microscopically, this is equivalent to realize "layer-by-layer" growth. By "layer-by-layer" growth we mean that the layer $n+1$ does not start to growth until the n-layer is completed.

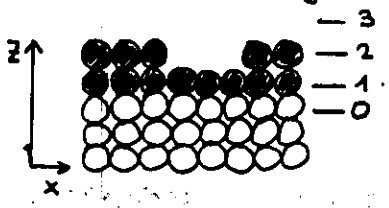

layer 3 does not start to grow until 2 is completed.

In metal epitaxy, what is more likely to occur is interdiffusion between adsorbed atoms and substrate atoms or clustering of the adsorbed atoms. Both these mechanisms give rise to "imperfect" interfaces and "imperfect" overlayers

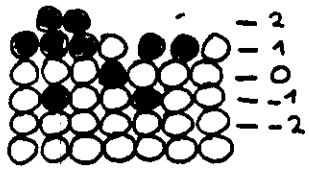

layer 2 is already populated while 1 is still incomplete. even layers 0 and -1 contain some atoms ●.

This occurs because the ideally flat overlayer is not necessarily the most stable thermodynamic configuration of the system substrate-adsorbate.

Consider an atom ● arriving at a surface during the growth of an epitaxial film. For the position this atom

can assume on such a surface there are several possibilities:

- the atom might stick within layer 1 in the vicinity of a similar atom ●. In this case, it would lower the energy of the system by restoring the bounds with some neighbours, which were severed in its absence. The energy associated with this process is $-|E_{LL}|$.
- There are however other possibilities to restore severed bonds:

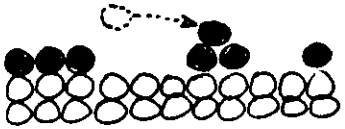

in this configuration, the number of restored bonds belonging to the adsorbed atoms is maximized, while no bonds belonging to substrate atoms are restored. The energy associated with this configuration is $-|E_c|$. This configuration might be energetically favoured if it costs less energy to expose one atom of the O-type than one atom of the type ● to the vacuum.
- A third possibility involves the incoming atom getting buried into the substrate, while a substrate atom

leaves the bulk. The energy associated with this "interdiffusion" process is $-|E_i|$.

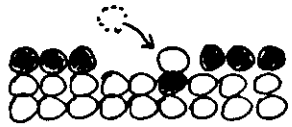

In this case, no new bonds of atoms of the ●-type is exposed to the vacuum, and this might be energetically more favoured.

Against layer-by-layer growth is certainly the requirement of maximizing the entropy, which is best realized by maximizing the number of "defects" of layer-by-layer growth. Let $n_c(n_i)$ the number of defects from "layer-by-layer" growth in thermodynamic equilibrium. The entropy $S_c(S_i)$ associated with these defects is roughly $\ln P_c$ ($\ln P_i$), where $P_c(P_i)$ is the number of possible positions $n_c(n_i)$ defects can assume within the N lattice positions within layer $O(2)$. According to the rules of statistics

$$P_\alpha = \frac{N!}{(N-n_\alpha)!\, n_\alpha!} = \binom{N}{n_\alpha} \qquad \alpha = c, i$$

. The change in free energy brought about by such defects is

$$\Delta F = \sum_{\alpha=i,c} \left[n_\alpha (E_{ll} - E_\alpha) - T \ln P_\alpha \right].$$

Using Stirling formula $\ln L! \simeq L \cdot \ln L - L$ we obtain

$$P_\alpha \cong N \ln N - N - \left[(N-n_\alpha)\ln(N-n_\alpha) - (N-n_\alpha)\right] - \left[n_\alpha \ln n_\alpha - n_\alpha\right] \sim N \ln N - (N-n_\alpha)\ln(N-n_\alpha) - n_\alpha \ln n_\alpha$$

so that $\Delta F = \sum_{\alpha=i,c} \left[n_\alpha (E_{ee} - E_\alpha) - T \left\{ N \ln N - (N - n_\alpha) \ln (N - n_\alpha) - n_\alpha \ln n_\alpha \right\} \right]$.

The number of equilibrium defects n_α is obtained from the equation $\frac{\partial \Delta F}{\partial n_\alpha} = 0$

which gives $\frac{n_\alpha}{N} = \frac{1}{1 + e^{(E_{ee} - E_\alpha)/T}}$

Depending on the values of E_{ee} and E_α ($\alpha = i,c$) - which, incidentally, nobody is able to calculate at present - and on the temperature at which epitaxy is performed - typically room temperature - there will be a certain number of defects from layer-by-layer growth in thermodynamical equilibrium.

From these thermodynamical considerations an element is still missing. Let us assume the experimental conditions are tuned so that the incoming atom is initially within the layer 1 - we will see soon how this can be realized in practice. Even if $|E_\alpha| > |E_{ee}|$ - i.e. layer-by-layer grow is not the thermodynamically most stable state - there will be an energy barrier on the way to the thermodynamically favoured configuration. Because of such barrier, $n_{\alpha/N}$ must be multiplied by $\omega_{mean} e^{-E_b/T}$,

where ω_{mean} is the mean phonon frequency at a given temperature and E_b is the height of the energy barrier. ω_{mean} can be estimated from the Einstein-Debye model for the lattice vibrations:

$$\omega_{mean} \sim \int_0^{\omega_{max}} \frac{\omega \cdot \rho(\omega)}{e^{\hbar\omega/kT} - 1} \Big/ \int_0^{\omega_{max}} \frac{\rho(\omega)\, d\omega}{e^{\hbar\omega/kT} - 1}$$, where

$\hbar \omega_{max} \sim k \cdot \Theta_{Debye}^{surface}$. With $x = \hbar\omega/kT \Rightarrow$

$$\omega_{mean} \sim \int_0^{x_{max}} \frac{(x \cdot T)^3 \cdot T\, dx}{e^x - 1} \Big/ \int_0^{x_{max}} \frac{(x \cdot T)^2 \cdot T\, dx}{e^x - 1} \sim T$$

For the "true" number of defects $n_{\alpha/N}$ from layer-by-layer growth we obtain

$$n_{\alpha/N} \sim \frac{T \cdot e^{-E_b/T}}{1 + e^{(E_{ee} - E_\alpha)/T}}$$

Some consequences of this equation are the following. Even if $E_{ee} - E_\alpha > 0$, there always are some defects at finite temperatures, because of the entropy. If $E_{ee} - E_\alpha < 0$, there will be an energy barrier to overcome, i.e $n_{\alpha/N} \sim T \cdot e^{-E_b/T}$. At sufficiently low temperatures, therefore, one might have in any case some amount of layer-by-layer growth. In fact, the above equation contain a very intuitive limiting case: for $T \to 0$

$n_{d/\eta} \longrightarrow 0$. This requirement of low temperatures favouring layer-by-layer growth clashes against the requirement of achieving an ordered overlayer (which is the case considered by most theories). This last requirement demands the temperature to be high enough so that the incoming atoms are given the possibility of locking into a lattice site, the same type of lattice sites for each adsorbed atom! Otherwise, bridge, top and hollow sites will be statistically occupied, giving rise to an homogeneous but disordered growth!

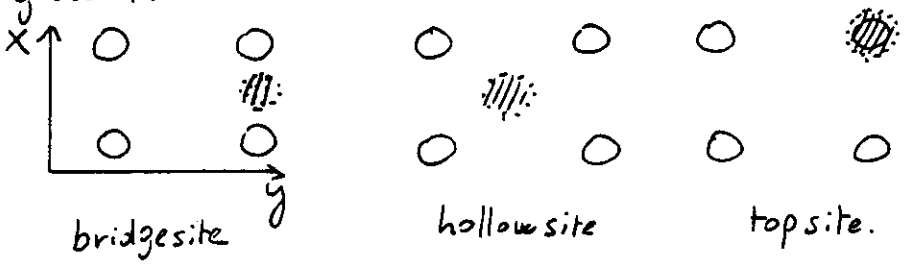

Summarizing: metal epitaxy is a very complicated process, which cannot at present be simulated even by the most powerful supercomputers. It is therefore left to the experiment to decide, whether a film consisting of atom X grows on a substrate of atoms y in a layer-by-layer mode or not. In section 1.3 we will consider some of the tools which allow the detection of layer-by-layer growth.
ordered

Before that, we will substanciate our claim that it is possible to chose experimental conditions so that the incoming atom is, initially, within the growing layer. To achieve this very important condition for layer-by-layer growth it is necessary that the mean distance between the atoms within the incoming beam is much larger than the lattice constant. In this way, the probability of too many incomig atoms arriving at the same place is minimized. Between the density n of the atoms in the incoming beam and the flux F there is the relationship $F = \frac{1}{4} n \cdot \bar{v} = \frac{1}{4} n \cdot \left(\frac{kT}{m}\right)^{1/2}$, where $\bar{v}$ is the mean velocity and T the temperature at which the beam is formed. Typical experimental conditions for Fe-deposition are $T \sim 1400\,K$ and one monolayer being formed every 250 sec on top of -say- Au (100). Because in metal epitaxy the sticking coefficient is ~ 1, we obtain $F \sim \frac{1}{(a)^2} \cdot \frac{1}{\tau}$ where a is the lattice constant and τ the deposition time. Apart from a numerical factor which we are going to calculate - $n \sim \frac{1}{\bar{r}}$ and the mean distance between the atoms $\bar{r}$ is $\sim r^3$. The deposition rate is therefore the crucial parameter entering the epitaxy process. It has to be very low,

in order for layer-by-layer growth to be optimized. On the other side, even in a vacuum of 10^{-10} Torr, the adsorbed film is likely to include 1ML of impurities every 10.000 sec, so that the time for the formation of a 1 ML-film has to be much lower than this. It turns out that $\tau \sim 250$ sec is high enough to induce layer-by-layer growth in the Fe/Au(100) system and low enough for the films to be very clean (< 1% contamination). Inserting the numbers corresponding to this experimental condition, we obtain $n \sim 8.5\ 10^{-16}$ $\frac{\text{atoms}}{\text{Å}^3}$

and a mean distance $\bar{r} \sim 2 \cdot 10^5$ lattice constants. This distance reduces of course dramatically (as τ^{-3}) upon increasing the deposition rate to the "typical" number 1 Å/sec ~ 0.5 ML/sec : $\bar{r}$ becomes $\ll 1$ lattice constant, i.e. under these conditions layer-by-layer growth is impossible. Notice that the "typical" deposition rate of 1 Å/sec is still commonly used in many laboratories: reports on metal epitaxy from these laboratories are to be regarded very skeptically !!

1.3. Growth detection

The problem is one of determining the spatial distribution of a very small amount of atoms (~ 10^{15} as opposed to 10^{23} in bulk) on top of a substrate. It is exquisitely a question for surface physics. In the past 20 years, this branch of Physics has developed a number of experimental techniques aimed at investigating the structure and the chemical composition of the top few surface layers. Most of them rely on detecting electrons ejected by some means (electron scattering, photoemission, ...) from the solid. Owing to the fact that electrons in the 10 eV - 1000 eV range have a very short mean free path before they lose part of their original energy by inelastic scattering processes, the probing depth of electron-based spectroscopies is only 2-6 top surface layers. For this reason, the detection of the film characteristics in metal epitaxy occurs mainly via electron based techniques.

The translational symmetry of the growing structure is best detected by looking at the diffraction pattern resulting from the elastic scattering of low energy electrons (LEED - Low Energy Electron Diffraction) - electrons with kinetic energy typically between 10 and 200 eV. For a 2d-array of atoms located at the lattice sites $\vec{R}_1, \ldots \vec{R}_j, \ldots \vec{R}_M$ the scattering

operator between the incoming electron and the surface atoms is $V = \sum_j W(\vec{r} - \vec{R_j})$. In the Born approximation – i.e. assuming the electron is scattered only once on its way to the detector – the scattering amplitude for an incoming plane wave $e^{i\vec{k_i}\cdot\vec{r}}$ is

$$\langle \vec{k_f} | V | \vec{k_i} \rangle = \sum_j \int e^{-i\vec{k_f}\cdot\vec{r}} W(\vec{r} - \vec{R_j}) e^{i\vec{k_i}\cdot\vec{r}} d^3r$$

$$= \sum_j e^{i(\vec{k_i} - \vec{k_f})\cdot\vec{R_j}} \cdot \underbrace{\int d^3(\vec{r} - \vec{R_j}) \cdot W(\vec{r} - \vec{R_j}) e^{i(\vec{k_i} - \vec{k_f})\cdot(\vec{r} - \vec{R_j})}}_{\widetilde{W}(\vec{k_i} - \vec{k_f})}$$

$$= \widetilde{W} \cdot \sum_j e^{i(\vec{k_i} - \vec{k_f})\cdot\vec{R_j}}$$

, where $\vec{R_j}$ is a lattice vector of the form $\vec{R_j} = (x_j, y_j, 0)$. This matrix element consists of the coherent sum of scattering amplitudes from each surface atom – as such interference effects are expected to occur. In fact, the scattering amplitude is zero unless the parallel component of $(\vec{k_i} - \vec{k_f})$ is not a reciprocal surface lattice vector, for which $(\vec{k_i} - \vec{k_f})_{\parallel} \cdot \vec{R_j} = \text{integer} \cdot 2\pi$, $\forall j$. Because of this selection rule, the diffraction pattern from an ordered array of atoms arranged in a plane consists of well defined narrow spots, which allow

a sharp picture of the reciprocal space to be obtained.

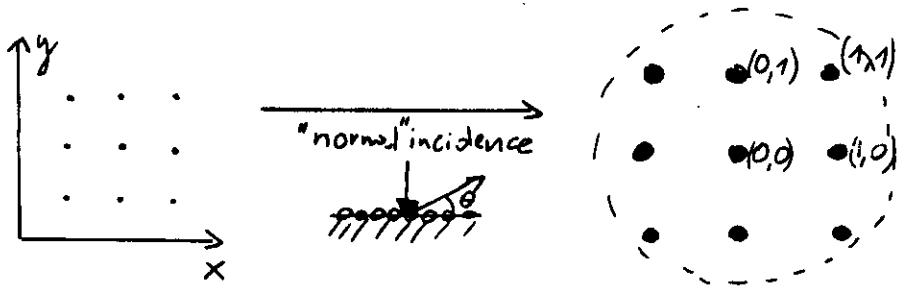

"real" space diffraction pattern.

For both the z-components k_{iz} and k_{fz} there are no selection rules except energy conservation: for normal incidence $\frac{\hbar^2 (k_{iz})^2}{2m} = E$ and $\frac{\hbar^2 G_{\parallel}^2}{2m} + k_{fz}^2 \cdot \frac{\hbar^2}{2m} = E = \frac{\hbar^2}{2m} G_{\parallel}^2 (1 + \sin^2\theta)$. From these equations it is evident that when E is varied the diffraction spot corresponding to a given $G_{\parallel}$ is always visible, albeit at a different observation angle θ: the diffraction pattern "moves" upon changing the energy. For $G_{\parallel} \neq 0$, the spot is no longer visible below a certain, well defined, energy: $\sin^2\theta < 0$ has no solution. Within this approximation, the intensity of the spots is only weakly modulated by the matrix element $\widetilde{W}$, which is a smooth function of E and θ. However, when the finite penetration depth is taken into account, we have interference

between waves scattered from difference surface planes.

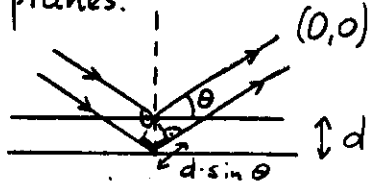

The waves scattered from the two surface planes are in phase (constructive interference) only for such energies $\frac{\hbar^2}{2m}\cdot\left(\frac{2\pi}{\lambda}\right)^2$ for which $2d\cdot\sin\theta = \text{integer}\cdot\lambda$

Upon changing the energy, the intensity of the various spots assumes maxima and minima: the energies for which such maxima occur are used essentially to measure d - the distance between the few top surface layers. This is particularly useful, for instance, in distinguishing between fcc-stacking of bcc-stacking of the adsorbed atoms. Both structures have the same surface translational symmetry, i.e. their diffraction patterns are undistinguishable. bcc and fcc stackings have identical surface nets, rotated by 45°. The next atom will arrive in the center of the surface unit cell, at a distance d above the surface layer. The only difference between fcc and bcc is that $d = a\cdot\sqrt{2}/2$ for fcc, while $d = a/2$ for bcc.

By measuring so called I-V (V: voltage = energy) curves is possible to distinguish between the two stackings.

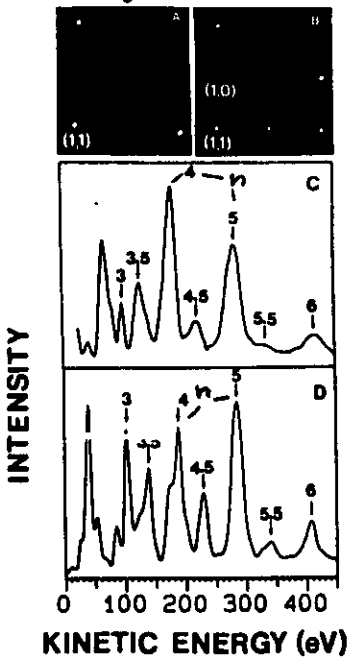

LEED pattern from a clean Cu(100)-surface (Fig. A) and from a 8 ML thick Fe-film deposited on the Cu(100)-surface (Fig. B). Common to both pattern is the square symmetry. The I-V curve (Fig. d) of the (00)-beam from the clean Cu(100)-surface shows maxima at $E_n = \frac{\hbar^2}{2m}\left(n\cdot\frac{2\pi}{a_\perp}\right)^2$, where $a_\perp$ is the well known lattice constant of the fcc-Cu. Bulk Fe is bcc, but the occurrence of intensity maxima of the (00)-beam from the epitaxial Fe (Fig. c) at the same energies as in Fig. d shows that the bcc-stacking for these Fe-films can be ruled out. Evidently, by epitaxying Fe on Cu-(100), the Fe atoms can be stabilized into the artificial fcc-structure, which is not present in nature. The physical realization of metastable crystal structures is one of the most exciting applications of metal epitaxy. (From Solid State Comm. 57, 329 (1986)).

A further application of the interference between different surface-planes are the so-called H(M)EED oscillations (H(M)EED: High (Medium) Energy Electron Diffraction). In the case layer-by-layer growth proceeds via nucleation of 2d-patches, there is the possibility of interference between terraces separated by one ML steps:

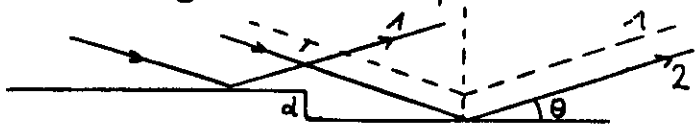

The condition for constructive (destructive) interference is $2d \sin\theta = n \cdot \lambda$ ($n/2 \cdot \lambda$). At a given θ, one can chose λ so that $2d\sin\theta = n/2 \cdot \lambda$. At the begin of growth, no patches are present, and the intensity of the reflected electrons is I_0. At 1/2 ML, 50% of the surface is covered by patches, which interfere destructively with the substrate: one expects $I_{1/2} < I_0$. At the 1 ML-stage, the I_0 value should be recovered. As a function of deposition time, the intensity I should show an oscillatory behaviour, with maxima corresponding to each layer being completed. The occurrence of oscillations during growth indicates that some amount of layer-by-layer growth is present and allows one to determine the thickness of the deposited layer.

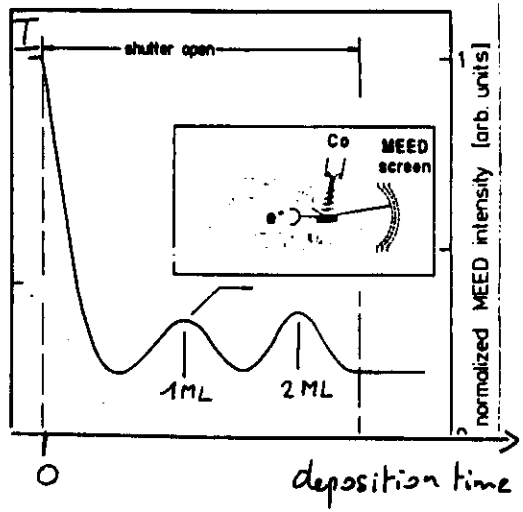

MEED oscillations detected during growth of Co on Cu(100), from J. Kirschner et al., Phys. Rev. Lett. 64, 1053 (1990).

An important parameter affecting the quality of metallic superlattices is the amount of impurities (O, S, N, C, ...) imbebbed in the layer. Such impurities may be adsorbed directly from the surrounding vacuum or may originate from the source of the metallic atoms. The method of detecting such impurities is Auger spectroscopy. When a monoenergetic (typically 3 keV) electron beam hits a surface, it forces a number of electrons to leave the surface. They are energetically distributed over a wide range:

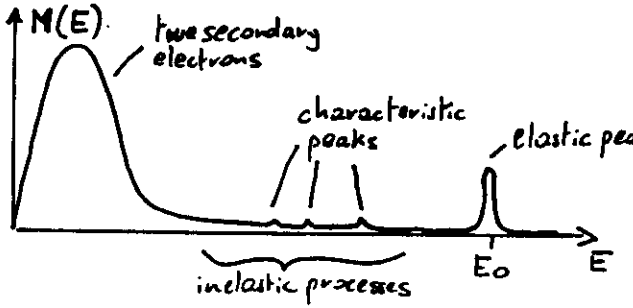

Auger electrons are among the "small" peaks in the inelastic energy range

The Auger-process is essentially an atomic one: it involves removing an electron from the core level

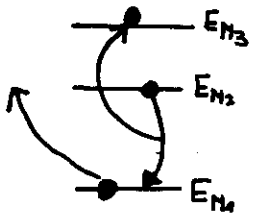

E_{N_1} by the incident electrons - filling the E_{N_1}-hole with an electrons "falling" from the E_{N_2}-level - ejecting an electron from the E_{N_3} level by a photon (or an electron) which carries the energy $E_{N_2} - E_{N_1}$. Essential of an Auger-process is that the kinetic energy of the Auger-electrons depends only on the relative position of $E_{N_1}, E_{N_2}, E_{N_3}$. Such core level energies are characteristic of each individual element, so that the kinetic energy of Auger electrons identifies almost univocally the presence of a certain element within the probing depth of Auger-spectroscopy. For instance, O has a strong Auger peak at about 513 eV, while Co and Cu have Auger peaks at higher energies. By following the intensity I_O of 513 eV-electrons during the growth of Co films on Cu (100), it is possible to determine how much O-free are such films. For a quantitative determination of the chemical composition at surfaces, one uses published Auger-cross sections A_α for the various elements. The concentration of the element α within a sheet containing the elements $i_1 \dots i_N$ is

then given by $C_\alpha = \dfrac{I_\alpha / A_\alpha}{\sum_{j=i_1,\dots,\alpha,\dots i_N} I_j / A_j}$,

provided the elements $i_1 \dots i_N$ are homogeneously distributed within the surface sheet.
(See, for an application of Auger-spectroscopy, Phys. Rev. Lett. 48, 645 (1982)).

A more subtle use of Auger-spectroscopy is the detection of layer-by-layer growth. Let i-layers of an epitaxial film being completed in a layer-by-layer growth fashion. Each layer $i, i-1, \dots 1$ consists of N atoms contributing an amount $I_\alpha \cdot e^{-(i-j)/\lambda}$ to the Auger current, $j = i, \dots, 1$ and λ the probing depth. The total Auger current from the already completed i-layers is $I_\alpha \cdot N \cdot \sum_{j=1,\dots,i} e^{(i-j)/\lambda}$.

When the $i+1$ layer is being formed, the newly arrived n_{i+1} atoms will contribute $I_\alpha \cdot n_{i+1}$ to the Auger current. The n_{i+1} atoms beneath them will contribute $I_\alpha \cdot n_{i+1} \cdot \left[\sum_j e^{-(i-j)\cdot\lambda}\right] \cdot e^{-1/\lambda}$. The remaining $(N - n_{i+1})$ atoms will contribute $(N - n_{i+1})\left[\sum_j \dots\right] I_\alpha$

The total current resulting during the formation of the $i+1$ layer is therefore

$$I_\alpha \cdot \left[n_{i+1} + (N - n_{i+1}) \cdot \sum_j e^{-(i-j)/\lambda} + n_{i+1} \cdot e^{-1/\lambda} \cdot \sum_j \dots \right]$$

Taking into account that $n_{i+1} = c \cdot t$, where c is the deposition rate, τ is the time for the completion of one ML – $N = c \cdot \tau$,

$$\sum_{j=1 \ldots i} e^{-(i-j)/\lambda} = \left(1 - e^{-i/\lambda}\right) / \left(1 - e^{-1/\lambda}\right)$$

the total current becomes

$$c \cdot t \cdot e^{-i/\lambda} + c \cdot \tau \cdot \frac{e^{-i/\lambda} - 1}{e^{-1/\lambda} - 1}$$, which

is – as a function of the deposition time – a straight line with slope $c \cdot e^{-i/\lambda}$, i.e. with decreasing slope when i increases. As a result, the Auger intensity plotted as a function of deposition time should be a succession of straight lines with abrupt change of slope at the completion of each monolayer. This "break" points should be equidistant, provided the deposition rate is kept constant.

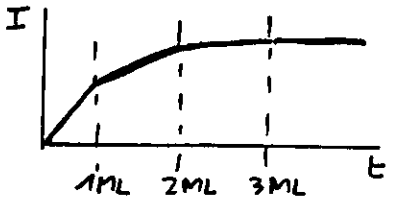

From such uptake curves the thickness of the film is easily obtained.

A textbook example of this method is given by R. Willis et al. in Surf. Sci. 187, 327 (1987) for the "ideal" epitaxial layer Co/Cu(100).

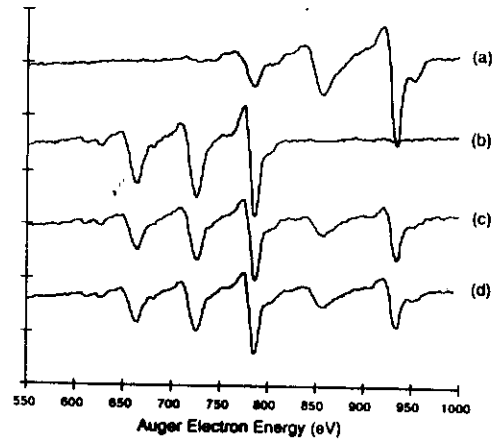

Fig. 1. Typical Auger spectra used in the fitting procedure to determine the signal strength from the cobalt relative to the substrate signal. Curves a and b show spectra taken from clean copper and a thick cobalt film respectively. These are used as reference spectra and any measured spectrum (curve c) is considered to be a linear superposition of the reference spectra. Such a superposition is shown by curve d.

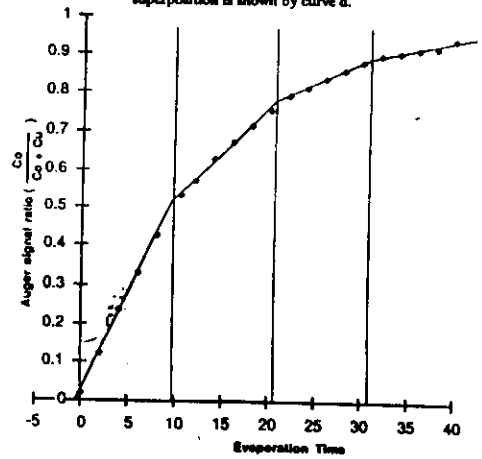

Fig. 2. Auger uptake curve for the growth of cobalt overlayers on the copper substrate. The fit to a layer-by-layer growth mode is shown.

To improve statistic, the whole "length" of the measured spectrum (c) is taken into account. The plot in Fig. 2 refers to the component Co in the linear superposition of the reference spectra.

2. The magnetic ground state of epitaxial layers.

One of the driving force behind metal epitaxy is the possibility of manufacturing new, artificial structures with extraordinary magnetic properties, unknown to our three dimensional world. An enormous effort is being done toward the physical realization of "perfect" epitaxial layers of the common bulk ferromagnets Fe, Co, Ni and Gd atop a non-magnetic substrate like noble metals (Cu, Ag, Au) or W. Some results we have seen in the first lecture: epitaxial layers of Co/Cu(100) and Fe/W(110) are very close to be "ideal" 2d-structures. The aim of this lecture is to explore the features of the ground state specific to such epitaxial layers.

The origin of the magnetic moment in atoms and in solid is the Coulomb-interaction between electrons centered around each atom. Consider, for instance, the 6 ($n=3, \ell=2$) electrons of an Fe atom (configuration: $3d^6$). The possible values for the total spin S are found by developing $(D^{1/2})^6$ into a Clebsch-Gordan serie ($D^{1/2}$: irreducible representation of SU_2 belonging to $s=1/2$). One finds $(D^{1/2})^6$ contains D^3, D^2, D^1 and D^0, i.e. $S = 3, 2, 1, 0$. These states are

degenerate when only the Coulomb interaction with the nucleous (appropriately screened by the core electrons) is considered, i.e. $H_0 = \sum_{i=1\ldots6} \frac{\vec{p}_i^2}{2m} + \sum_{i=1\ldots6} Z\cdot\varepsilon\cdot e^2/|\vec{r}_i|$. All spin states $S=3,2,1,0$ belong to the same eigenvalue E_0, which is 2^6 degenerate. This degeneracy is generally lifted by the Coulomb interaction between the electrons: $H' = \frac{1}{2}\sum_{i,j} e^2/|\vec{r}_i - \vec{r}_j|$. This is the content of a theorem by P.A.M. Dirac. Upon switching on H', the first order perturbation theory correction to the eigenvalue E_0 is given by the eigenvalues of the matrix H', with $H'_{pq} = \langle p|H'|q\rangle$ and $|p\rangle, |q\rangle$ one of the 2^N states within the eigenspace of E_0. Dirac was able to show that the eigenvalue problem of H' in the orbital eigenspace $\{|p\rangle\}$ is equivalent to the eigenvalue problem of the following Hamiltonian in spin space:

$$H'_S = C\cdot\mathbb{1} - \frac{1}{2}J_{ex}\cdot\sum_{i,j}\left(\vec{\sigma}_i\cdot\vec{\sigma}_j + 1\right)$$

where $\vec{\sigma}_i, \vec{\sigma}_j$ are Pauli matrices. C is the so called Coulomb integral, $C = \int Y^*_{\ell m'}(\vec{r}_2)\cdot Y^*_{\ell m}(\vec{r}_1)\frac{e^2}{|\vec{r}_1-\vec{r}_2|}\cdot Y_{\ell m'}(\vec{r}_2)\cdot Y_{\ell m}(\vec{r}_1)$ and represent the Coulomb energy between two charges $|Y_{\ell m'}(\vec{r}_2)|^2$ and $|Y_{\ell m}(\vec{r}_1)|^2$. J_{ex} is the so called exchange integral and arises from the indistinguishibility of electrons:

$$J_{lm} = \int \psi^*_{e'm'}(\vec{r}_2)\cdot\psi^*_{em}(\vec{r}_1)\cdot\frac{e^2}{|\vec{r}_1-\vec{r}_2|}\cdot\psi_{e'm'}(\vec{r}_1)\cdot\psi_{em}(\vec{r}_2)$$

Generally J_{Hu} is positive and forces the true ground state to have the highest spin S compatible with the requirement that two equal spins cannot have the same orbital wave function (so called 1. Hund'rule, this is why we use the symbol J_{Hu}).

$3d^6$

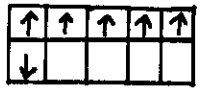

$l = 2\ 1\ 0\ -1\ -2$

The ground state configuration of Fe arising from the 1. Hund's rule is the one with $S=2$, i.e. with magnetic moment $\mu = 2\cdot\mu_B\cdot S = 4\mu_B$. J_{Hu} is typically 1-5 eV for d-electrons: this means that the state with $S=1$ lies by this energy amount above the groundstate.

Having established that the origin of the magnetic moment is an atomic one, we ask next what happens when the magnetic moment is immersed into a "see" of conduction electrons. This question is fundamental in understanding the evolution of the magnetic moment when atoms are brought together to form a solid. For our purposes, we consider 2 p-electrons, with a two-level configuration $S=1$ and $S=0$. If isolated, these two levels are split by an amount J_{Hu} and there is no matrix element between them. When

in contact with a plane wave electron the Coulomb interaction $\frac{e^2}{|\vec{r}_3-\vec{r}_2|}+\frac{e^2}{|\vec{r}_3-\vec{r}_1|}$ between the plane wave electron at $\vec{r}_3$ and the atomic electron $\vec{r}_2$, $\vec{r}_1$ introduces non-vanishing matrix elements $\langle\vec{k}|\sum_{i=2,1}\frac{e^2}{|\vec{r}_3-\vec{r}_i|}|1\rangle$ and

$$\langle\vec{k}|\sum_{i,j,1}\frac{e^2}{|\vec{r}_3-\vec{r}_2|}|0\rangle .$$

For the two level atomic system, the existence of such matrix elements means that $|1\rangle$ and $|0\rangle$ has now the chance to intermix: the eigenvalue problem within the atom becomes

$$\begin{pmatrix} E_1 & \lambda \\ \lambda & E_0 \end{pmatrix} \psi = E\psi \ , \text{ where the}$$

size of λ is essentially a measure of the hybridization between the atomic wave functions and the plane wave electron. As a result of the switching on of λ, the "new" atomic wave functions will be a linear superposition of $|1\rangle$ and $|0\rangle$, with

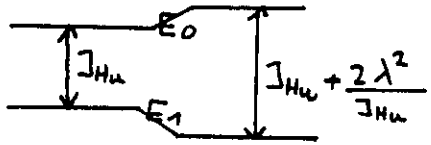

the energy levels split further apart. Any linear combination of $|1\rangle$ and $|0\rangle$ will have $\langle S\rangle < 1$, so that the net result of the contact between atoms

and plane wave electrons is a reduction of the magnetic moment!! Notice that there is evidently a gain in energy associated with this reduction: the ground state is lowered by $\sim \lambda^2/J_{Hu}$. On the other hand, a reduction of μ tends to reduce the exchange splitting, raising again the value of the ground state energy. Whether magnetic moment will the atom assume in the solid depends on the balance of these two energies: in general, 4d and 5d transition metal wave functions are less localized than 3d-wave functions. The matrix element with conduction electrons is so large with respect to J_{Hu} that they loose their magnetic moment completely. By 3d-wave functions, though reduced, μ survives. The reduction from the atomic value is the more important, the longer is λ. In epitaxial monolayers, some of the nearest neighbours are missing, which is likely to reduce λ. By contrast, the contact with a non-magnetic substrate is likely to increase λ. The exact value depend on minute details of the electronic structure. As a result of a major computational effort by Freeman and coworkers, involving the most powerful supercomputers known to mankind, the following inequality has been established for most materials (with 3d-wave functions)

$$\mu_{atom} > \mu_I > \mu_{II} > \mu_{III} > \mu_{bulk}$$

For instance $\mu^{Fe}_{atom} = 4\mu_B$

$\mu_{1\,Fe/Au(100)} \sim 3\mu_B$ but

$\mu_{1\,Fe/W(110)} \sim 2.2\mu_B$

$\mu^{Fe}_{bulk} \sim 2.2\mu_B$

Experimental evidence to this picture is still missing.

The survival of the magnetic moment for each atom of a solid or an epitaxial monolayer does not imply the solid showing any magnetic properties at all on a macroscopic level. Consider the simple case of three hydrogen atoms put together to form a 2d-ring. Each atom carry spin 1/2, the ground state of $\sum_i \frac{p_i^2}{2m} + \sum_i \frac{e^2}{|\vec{r}_i - \vec{R}_i|}$ being highly degenerate with respect to $(D^{1/2})^3 = D^{3/2} + 2D^{1/2}$. Again, only upon switching on the Coulomb interaction between electron centered at different atoms will this degeneracy between $S = 3/2$ and $S = 1/2$ be lifted. The ground state energy of the hydrogen ring will result by solving the eigenvalue problem of the operator $H'_S = C - \frac{1}{2} J \sum_{i,j} (1 + \vec{\sigma}_i \cdot \vec{\sigma}_j)$, where J is the <u>interatomic</u> exchange integral. In general, J is of the order of 10^{-2}eV-

i.e. $J \ll J_{Hu}$ (so fast decreases J with distance!). Because of this interaction the groundstate can display the highest spin possible - which occurs when the spins are all aligned. It is this interatomic link between the individual magnetic moments which finally establish long range magnetic order in the groundstate. The Hamilton operator $H'_S = -\frac{1}{2} J \cdot \sum_{i,j}{}' (1 + \vec{\sigma_i} \cdot \vec{\sigma_j})$ is known as Heisenberg operator. Its non-trivial part is often generalized to $H' = -J \sum_{i,j} \vec{S_j} \cdot \vec{S_i}$.

We would like to give this operator a closer numerical inspection, with the aim of studying its full energy spectrum (including the excited states). These excited states lie above the ground state by only an energy amount of the order of J. Because of its small value, the excited states of the Heisenberg-Hamiltonian can be effectively populated at "reasonable" temperatures ($T < 1000$ K). This is in clear contrast with the excited states of the Hund's-Hamilton operator, which lie above the ground state by as much as 10^4-10^5 K!!

For numerical simplicity we limit ourselves to the ring of three hydrogen atoms, which, despite being very unrealistic, it displays all the essential features we want to point out.

The eigenvalue problem involves solving the determinantal equation of a $2^3 \times 2^3$ matrix $\langle m_3, m_2, m_1 \left| -\frac{J}{4} \cdot \sum_{\substack{i=1..3 \\ j=1..3}} \vec{\sigma_i} \cdot \vec{\sigma_j} \right| m'_3, m'_2, m'_1 \rangle$, where $m_j = |\uparrow\rangle$ or $|\downarrow\rangle$. Typically, only nearest neighbours interaction is considered, i.e. $\sum_{\substack{i \dots \\ j \dots}} \vec{\sigma_i} \cdot \vec{\sigma_j}$ reduces to $\vec{\sigma_1} \cdot \vec{\sigma_2} + \vec{\sigma_2} \cdot \vec{\sigma_3} + \vec{\sigma_3} \cdot \vec{\sigma_1} + \vec{\sigma_2} \cdot \vec{\sigma_1} + \vec{\sigma_3} \cdot \vec{\sigma_2} + \vec{\sigma_1} \cdot \vec{\sigma_3}$. Moreover $\vec{\sigma_i} \cdot \vec{\sigma_j} = \vec{\sigma_j} \cdot \vec{\sigma_i}$ so that $-\frac{J}{4} \sum_{\dots} \dots = -\frac{J}{2} \cdot (\vec{\sigma_1} \cdot \vec{\sigma_2} + \vec{\sigma_2} \vec{\sigma_3} + \vec{\sigma_3} \cdot \vec{\sigma_1})$.

Group theory tells us that, because $(D^{1/2})^3 = D_{3/2} + 2 \cdot D_{1/2}$, the $2^3 \times 2^3$ matrix will reduce to

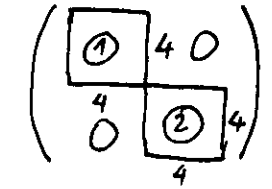

where the first block will contain eigenvectors transforming according to $D_{3/2}$ upon SU_2-transformation and block (2) as $D^{1/2}$. The eigenvalues of block 1 will be clearly $-3\frac{J}{2}, -3\frac{J}{2}, -3\frac{J}{2}, -3\frac{J}{2}$, i.e the groundstate is 4 times degenerate, corresponding to $S_z^{3/2} = 3/2, 1/2, -1/2, -3/2$. This ultimate degeneracy - a mere consequence of the rotational invariance of the Hamilton operator of N-electrons - means that systems with Heisenberg hamiltonian will never show any magnetic effect. We will later see that magnetism occurs when H' is supplemented by an external magnetic field $\vec{H}$.

· $\sum_i g \cdot \mu_B \cdot \vec{S_i}$ and M is defined as $\lim_{h \to 0} M(\vec{h})$.

(this means that, when calculating magnetic properties with H', one has to be very careful in not getting a wrong result only because one is not considering this difficulty). For our limited purposes, we will assigne a magnetic moment $3\mu_B$ to the groundstate of a ring of 3 hydrogen atoms.

Clearly, the 4 eigenvalues of block 2 belong to excited states of the system. For the same reason as the groundstate, we conclude that each eigenvalue of block 2 is twice degenerate. ($S_z = \pm 1/2$). By using all possible states $|m_1, m_2, m_3\rangle$ with $S_z = +1/2$ we are sure to built the smallest matrix containing the 2 eigenvalues we are looking for. Those states are, pictorially

$|1\rangle$ ↓ $|2\rangle$ ↑ $|3\rangle$ ↑

↑ ↑ ↓ ↑ ↑ ↓ We obtain a 3×3 matrix, but this does not surprise us: one linear combination of $|1\rangle, |2\rangle, |3\rangle$ belongs certainly to $S_z = 1/2$ but $S = 3/2$!! At this point, what is left to do is to setup a 3×3 matrix and solve the determinant $|H' - E| = 0$, knowing that on solution for E is certainly $-3\frac{J}{2}$. Very easy. But we want to complicate slightly the solution, with the aim of finding a more

suggestive way of representing the results! We want to point out a further symmetry of the problem, arising from the atoms being arranged into a closed chain rather than on an open-ended one. Because of this "boundary" condition - reminescent of the Born-von Karman cyclic boundary conditions in solids - the cyclic group of permutations $\begin{pmatrix}1&2&3\\1&2&3\end{pmatrix}$ $\begin{pmatrix}1&2&3\\2&3&1\end{pmatrix}$, $\begin{pmatrix}1&2&3\\3&1&2\end{pmatrix}$ is also a symmetry group of the Hamiltonian. This fact can be used to solve the eigenvalue problem of the 3×3 matrix. A pictorial representation of the elements of this group is as follows:

$\begin{pmatrix}1&2&3\\1&2&3\end{pmatrix}$ $\begin{pmatrix}1&2&3\\2&3&1\end{pmatrix}$ $\begin{pmatrix}1&2&3\\3&1&2\end{pmatrix}$

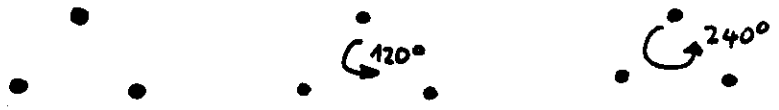

This group is commutative so that each irreducible representation is 1 dimensional. A suitable way to represent this group is the use of a quantity K which is the equivalent of the wave-vector arising from the Born-von Karman boundary conditions. One can write the character table (which coincide, in the present case, with the representations themselves) as follows:

	0	+120°	240°
C_0	1	1	1
C_1	1	$e^{ik_1\cdot 1}$	$e^{ik_1\cdot 2}$
C_2	1	$e^{ik_2\cdot 1}$	$e^{ik_2\cdot 2}$

$k_1 = 2\pi/3 \cdot 1$

$k_2 = 2\pi/3 \cdot 2$

To find the eigenvectors of C_0, C_1, C_2 we use the formula

$$\chi_i = \sum_{g\in G} C_i(g)\cdot \chi \text{ , where } \chi \text{ is}$$

some vector in the eigenspace of the 3×3 matrix. ($\chi = (1,1,1)$). Using this group theoretical help, we find the eigenvector of H to be

$(1,1,1)$ $(1, e^{ik_1\cdot 1}, e^{ik_1\cdot 2})$ $(1, e^{ik_2\cdot 1}, e^{ik_2\cdot 2})$

C_0 C_1 C_2

without even solving a determinantal equation (in fact, without even knowing the matrix!).

For setting up the matrix we make good use of the following table: (Feynman lectures, vol. III).

$\sigma_0^i\sigma_0^j|+\,+\rangle = +|-\,-\rangle$
$\sigma_0^i\sigma_0^j|+\,-\rangle = +|-\,+\rangle$
$\sigma_0^i\sigma_0^j|-\,+\rangle = +|+\,-\rangle$
$\sigma_0^i\sigma_0^j|-\,-\rangle = +|+\,+\rangle$

$\sigma_0^i\sigma_0^j|+\,+\rangle = -|-\,-\rangle$
$\sigma_0^i\sigma_0^j|+\,-\rangle = +|-\,+\rangle$
$\sigma_0^i\sigma_0^j|-\,+\rangle = +|+\,-\rangle$
$\sigma_0^i\sigma_0^j|-\,-\rangle = -|+\,+\rangle$

$\sigma_0^i\sigma_0^j|+\,+\rangle = +|+\,+\rangle$
$\sigma_0^i\sigma_0^j|+\,-\rangle = -|+\,-\rangle$
$\sigma_0^i\sigma_0^j|-\,+\rangle = -|-\,+\rangle$
$\sigma_0^i\sigma_0^j|-\,-\rangle = +|-\,-\rangle$

e, p means i, j: actually $\vec{\sigma}_i\cdot\vec{\sigma}_j$ act on $|m_s^1, m_s^2, m_s^3\rangle$ where $m_s^i = \uparrow$ or $\downarrow$ (+ or −), but only the components i, j are affected. After some simple algebra one finds

$$H' = \begin{pmatrix} J/2 & -2J/2 & -2J/2 \\ -2J/2 & J/2 & -2J/2 \\ -2J/2 & -2J/2 & J/2 \end{pmatrix}$$

Inserting the eigenvector $(1,1,1|$ in $(H'-E)\chi = 0$, which belong to the representation C_0, one finds the equation for E_0: $J/2 - E_0 - 4J/2 = 0$ i.e. $E_0 = -3J/2$. The vector $|\downarrow\uparrow\uparrow\rangle + |\uparrow\downarrow\uparrow\rangle + |\uparrow\uparrow\downarrow\rangle$ belongs to the ground state $(S^{3/2}_{+1/2})$. Inserting the vector $(1, e^{ik_1}, e^{i2k_1})$ one find the equation for E_1: $J/2 - E_1 - 2J/2\cdot e^{ik_1} - 2J/2\cdot e^{i2k_1} = 0$

Noticing that $e^{i2k_1} = e^{-ik_1}$ one finds the solution

$$\underline{E_1 = J/2 - 2J\cdot\cos k_1 .}$$

Moreover $\underline{E_2 = J/2 - 2J\cdot\cos k_2 = E_1 = 3J/2 > -3J/2.}$

E_1, E_2 are the excited states of the spin-ring and coincide. The full energy spectrum can be summarized as follows:

	k=0	k_1	k_2
$S=3/2$	$-3J/2$		
$S=1/2$		$3J/2$	$3J/2$

It is instructive to write further $E_1 - E_0 = 2J(1-\cos k_1) = 2J\cdot(1-\cos\frac{2\pi\cdot 1}{N})$

Such an expression is also correct for $N\gg 1$, in which case the energy of the first excited states can be written as $D\cdot k^2$, $K\ll 1$. For $N\to\infty$ the energy of the lowest excited states is arbitrarily close

to the ground state. At sizeable temperatures (room temperature) such excited states are generally occupied, so that they will play an essential rôle in the thermodynamic of the system. Such states, which lower the total spin of the system by 1, are the so called <u>spin wave (magon) states</u>, first discovered by F. Bloch.

In general, of relevance for the magnetic behaviour at finite temperatures are primarily (at least at low temperature) such excitations which involves lowering the total spin of the system by 1. From what we have learned so far, we are able to classify such states with respect to the ground state for 1 atom, N atoms, bulk ($N \times N \times N \to \infty$) and an epitaxial layer ($N \times N \to \infty$).

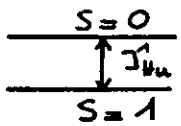

In an atom, the only possibility to lower the ground state magnetic moment is to occupy the non-magnetic state S=0 which lies J^{1}_{Hu} above the ground state. At reasonnable temperature, this excitation is not observed.

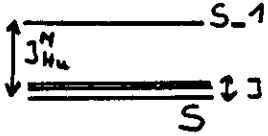

For a system consisting of N atoms a new channel is open to reduce the total spin by 1: the excitation into spin wave states, which cost much more less energy

than destroying the magnetic moment of an individual atom ($J < J^{N}_{Hu}$). Notice that, in general, $J^{N}_{Hu} < J^{1}_{Hu}$, although the reduction is not large enough to bring J^{N}_{Hu} in the range of J.

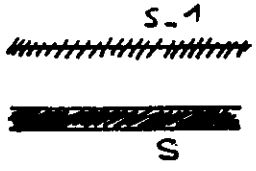

In a bulk, the spin wave states form close energy levels arbitrarily close to the ground state. Because of hybridization, there is also a broadening of the excited S-1 state, which remains far above the ground state, despite $J^{bulk}_{Hu} < J^{1}_{Hu}$. The only qualitative difference between bulk and epitaxial layer is that $\overline{J^{1}_{Hu}} > \overline{J^{bulk}_{Hu}}$. The excitation which lower S of an individual atom by 1 are called, in solid, <u>Stoner excitations</u>. With the exception of Ni, such excitations play a minor role in the thermodynamic of the system. Ni is an exceptional case where J^{Ni}_{Hu} is not far larger than J. In this case, one cannot treat the spin wave states and the S-1 local state separately: the true excited states spectrum is a linear combination of Stoner excitation and spin wave states. This makes Ni so difficult to be handled numerically. While Stoner excitation are not playing an important role for the finite temperature magnetic properties, they are known to exist from electron scattering. (J. Kirschner, Surf. Sci. 162, 83 (1985).

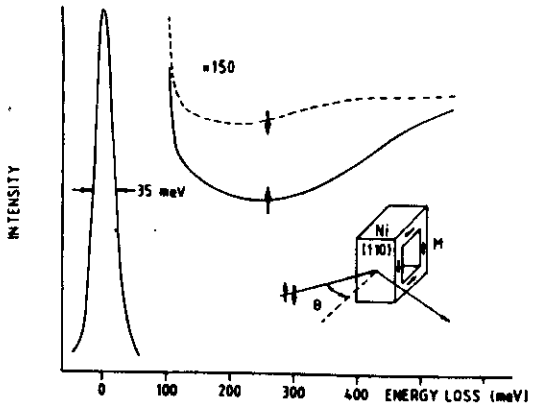

Fig. 3. Result of a high-resolution spin-polarized electron energy loss experiment on Ni(110). The arrows on the loss spectra refer to the primary electron spin orientation: ↑ antiparallel to the magnetization, ↓ parallel to the magnetization. The experimental geometry is sketched in the insert.

From J. Kirschner, Surf. Sci. 162, 83 (1985).

The intensity of the specularly reflected electrons is measured as a function of their energy loss and for the two spin orientations. The Fig. shows that the loss intensity when using primary electrons with spin opposite to the magnetization is larger than for primaries with their spin along M. This is because there is an excitation channel which works better for on type of electrons than for the other. The $3d^9$ configuration of Ni gives a clue to this asymmetric excitation:

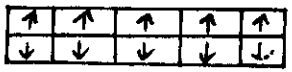

Only spin down electrons are able to lose their energy by exciting a Ni-atom into the $S=0$ state - Stoner excitation. For spin-up electrons this loss channel is not open.

3. The magnetism of epitaxial layers at finite Temperatures.

The $D\cdot k^2$ relationship is the key result for the understanding of magnetism at finite temperatures in epitaxial layers. The simplest model showing all the relevant (and curious) features of 2d-magnetism is the planar model, for which $H' = -J\cdot\sum_{i,j}\left[S_i^x\cdot S_j^x + S_i^y\cdot S_j^y\right]$. The analysis can be enormously simplified by giving up the quantum nature of the spins and simply substituting them with classical vectors. This step is justified in view of the spin-wave spectrum carrying no sign of the quantized nature of the individual spins. Moreover, since the thermodynamic is determined by large scale fluctuations, with characteristic length $1/k \gg$ lattice constant, a continuum limes is usually performed to suit the physical conditions. Writing $\vec{S}(\vec{x})$ as a classical vector $S\cdot\left(\cos w(\vec{x}), \sin w(\vec{x})\right) = S\cdot\vec{m}(\vec{x})$ the Hamiltonian becomes

$$-JS^2\sum_{\vec{x},\vec{a}}\vec{m}(\vec{x})\cdot\vec{m}(\vec{x}+\vec{a}) = -J\cdot S^2\cdot\sum_{\vec{x},\vec{a}}\cos\left(w(\vec{x})-w(\vec{x}+\vec{a})\right)$$

$$= -J\cdot S^2\cdot\sum_{\vec{x},\vec{a}}\cdot\sum_n(-1)^n/(2n)!\cdot\left(w(\vec{x}+\vec{a})-w(\vec{x})\right)^{2n}.$$

When only long wave length fluctuations are considered, the Hamiltonian can be approximated by

$$+\frac{J\cdot S^2}{2}\cdot\sum_{\vec{x},\vec{a}}\left(w(\vec{x}+\vec{a})-w(\vec{x})\right)^2 \quad \text{(spin wave or}$$

harmonic approximation. To perform the continuum limes $\omega(\vec{x}+\vec{a}) = \omega(\vec{x}) + \vec{\nabla}\omega \cdot \vec{a}$ and

$$\sum_{\vec{a}} (\vec{\nabla}\omega \cdot \vec{a})^2 = (a \cdot \vec{\nabla}\omega \cdot (1,0))^2 + (a \cdot \vec{\nabla}\omega \cdot (0,1))^2 + (a \cdot \vec{\nabla}\omega (-1,0))^2 + (a \cdot \vec{\nabla}\omega \cdot (0,-1))^2$$

$$= a^2 \cdot (\vec{\nabla}\omega)^2 \cdot (\sin^2\varphi + \cos^2\varphi) \cdot 2 = 2a^2 (\vec{\nabla}\omega)^2 .$$

$\sum_i \to \int dx^2$

so that $H = \frac{1}{2} \tilde{J} \cdot \int (\vec{\nabla}\omega)^2 d^2x \quad , \tilde{J} = \frac{1}{2} \cdot z \cdot S^2 J .$

Inserting for ω the Fourier-transform $\omega(\vec{x}) = \frac{1}{\sqrt{V}} \cdot \sum_k e^{i\vec{k}\cdot\vec{x}} \omega_k$ we obtain H in the Fourier representation:

$$H = \frac{1}{2} \tilde{J} \int \vec{\nabla}\left(\frac{1}{\sqrt{V}} \sum_k e^{ikx} \omega_k\right) \cdot \left(\vec{\nabla} \frac{1}{\sqrt{V}} \sum_{k'} e^{-ik'x} \overline{\omega_{k'}}\right) d^2x =$$

$$= \frac{1}{2} \tilde{J} \cdot \frac{1}{V} \underbrace{\int e^{ikx} \cdot e^{-ik'x} d^2x}_{V \cdot \delta_{kk'}} \cdot \sum_{k,k'} i \cdot k \cdot (-ik') \cdot \omega_k \cdot \overline{\omega_{k'}} =$$

$$= \frac{1}{2} \tilde{J} \sum_k \vec{k}^2 \cdot |\omega_k|^2 .$$

According to the rules of statistics, this Hamiltonian can be used to calculate all the relevant thermodynamic quantities. For instance

$$\langle |\omega_k|^2 \rangle = \frac{\int d\omega_{k_1} \dots d\omega_{k_N} \cdot |\omega_k|^2 \cdot e^{-\frac{1}{2}\tilde{J}/T \cdot \sum_{k_1 \dots k_N} k_i^2 \cdot |\omega_{k_i}|^2}}{\int d\omega_{k_1} \dots d\omega_{k_N} \cdot e^{-\frac{1}{2}\tilde{J}/T \cdot \sum_{k_1 \dots k_N} k_i^2 \cdot |\omega_{k_i}|^2}}$$

being $\int d\omega_{k_1} \dots d\omega_{k_N} \cdot e^{-\frac{1}{2}\tilde{J}/T \sum_i k_i^2 \cdot |\omega_{k_i}|^2}$ the partition sum.

Noticing that $\int \dots e^{\sum \dots} = \prod_{k_i} \int d\omega_{k_i} \cdot e^{\dots k_i}$

we obtain

$$\underline{\langle |\omega_k|^2 \rangle} = \left(\int d\omega_k \cdot |\omega_k|^2 \cdot e^{-\frac{1}{2}\frac{\tilde{J}}{T} k^2 |\omega_k|^2} \right) \Big/ \left(\int d\omega_k \cdot e^{-\frac{1}{2}\frac{\tilde{J}}{T} k^2 |\omega_k|^2} \right)$$

$$= \frac{\sqrt{\pi} \cdot T^{3/2}}{4 \cdot (\tilde{J}/2 \cdot k^2)^{3/2}} \Big/ \frac{\sqrt{\pi} \cdot T^{1/2}}{2 (\tilde{J}/2 \, k^2)^{1/2}} = \underline{\frac{T}{\tilde{J} \cdot k^2}}$$

In a 2d-planar system, the mean square deviation caused by spin wave like excitation is as follows:

$$\langle \omega(\vec{x})^2 \rangle = \frac{1}{V} \cdot \sum_k \langle |\omega_{\vec{k}}|^2 \rangle \Rightarrow \frac{1}{V} \cdot \frac{V}{(2\pi)^2} \int d^2k \langle |\omega_k|^2 \rangle =$$

$$= \frac{1}{(2\pi)^2} \cdot 2\pi \int_{2\pi/L}^{\frac{2\sqrt{\pi}}{a}} dk \, \frac{T}{\tilde{J} \cdot k^2} \cdot k = 2 \cdot \frac{T}{4\pi\tilde{J}} \cdot \ln L/a \; ,$$

where L is the linear dimension of the system.

The mean value of the magnetization $S \cdot \langle e^{i\omega(\vec{x})} \rangle$ can be calculated from $\langle \omega(x)^2 \rangle$ using a well known theorem of thermal averages with a Gaussian distribution: $S \cdot \langle e^{i\omega(\vec{x})} \rangle = e^{-\frac{1}{2}\langle \omega^2(\vec{x}) \rangle} \cdot S$

$$\Rightarrow \langle S \cdot e^{i\omega(\vec{x})} \rangle = S \cdot \left(\frac{L}{a}\right)^{-\Delta} \quad , \Delta = \frac{T}{4\pi\tilde{J}} .$$

(it is convenient to single out the quantity Δ, which will become later a relevant physical quantity).
At finite temperatures, long range order disappear in the thermodynamic limes $L \to \infty$. This is only true as long as $T > 0$: for $T = 0$ (= ground state) a net magnetization might exists. The no long range rule for 2d-systems with component n of the spin ≥ 2 is the content of the famous Mermin-Wagner theorem. Magnetism should not exist in 2d. Experimentally, however, long range order is observed at finite temperatures for epitaxial films as thin as 1 ML. Either such structures are not 2d-ones or something is missing in the Hamiltonian, which stabilizes long range order. We will show that the second alternative accounts well for the experimental evidence.
We summarize as follows the experimental evidence.

pendicular domains. In the present paper we measure the in-plane magnetization of 1 ML of Co on Cu(100) as a function of the applied magnetic field using the magneto-optical Kerr effect. We find the following: (a) 1 ML of Co on Cu has a square hysteresis loop; i.e., long-range ferromagnetic order exists at finite temperatures, over macroscopic size (precisely the size of the laser spot used for the measurements, ~ 3 mm^2) and in the absence of magnetic fields. (b) The spins lie in the film plane. This represents a clear and definite answer to the important question of perpendicular versus in-plane magnetization for a system whose perfection makes it a test case of the most advanced total-energy calculations on magnetic anisotropy (see, for instance, Ref. 5).

The experimental technique used to measure the magnetization is based on the magneto-optical Kerr effect. The possibility of using the Kerr effect in ultrahigh-vacuum experiments to measure the magnetization of very thin films was first demonstrated by Bader and Moog.[9] Here we use the *transversal* (or equatorial) Kerr effect: The plane including the surface normal and the incident and reflected light beams is perpendicular to the applied magnetic field. The magnetic field is *applied in the film plane*. The polarization of the light—a He-Ne laser—is parallel to this plane (p polarized light). In this geometry, the *reflected intensity* depends on the magnetic state of the sample[10]; i.e., by our sweeping the magnetic field the hysteresis loop can be recorded. Figure 1 shows the hysteresis loop recorded for the 1 ML of Co on Cu(100) at room temperature. The thickness was determined from Auger spectroscopy with use of the calibration curve published in Ref. 8. Similar hysteresis loops were measured up to 10 ML. No magnetic signal was observed for 0.6 ML. The main features of the hysteresis loop in Fig. 1 are the following:

(1) The magnetization M_R at remanence ($H = 0$) is equal, to within experimental accuracy, to the saturation magnetization; i.e., the monolayer is in a single-domain state at $H = 0$. This establishes unequivocally the existence of long-range order over macroscopic dimensions for a monatomic film. Moreover, apart from giving essential information on the magnetic state of the system, the observation of a square hysteresis loop adds to the evidence for epitaxial growth based on Auger and LEED spectroscopy,[8,16,17] the fascinating "magnetic" evidence of the 1 ML being so perfect that, after the field is removed, it survives in a single-domain state of macroscopic size!

(2) The magnetization reversal ($H < 0$) does not occur abruptly at a certain field: The magnetization changes continuously between $+M_R$ and $-M_R$. Therefore coherent rotation or displacement of one single macroscopic domain wall can be excluded. Instead, the film splits up into domains carrying $+M_R$ or $-M_R$, the numbers of which are exactly equal at $H_C \simeq -20$ Oe, where the resulting macroscopic magnetization disappears.

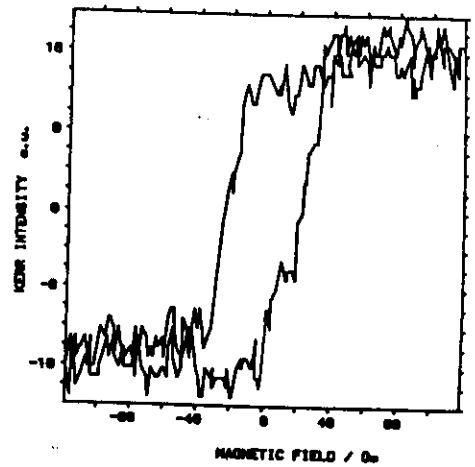

FIG. 1. Hysteresis loop for 1 ML of cobalt on Cu(100), averaged over twenty rapid field scans. The magnetic field, provided by two Helmholtz coils placed directly in the vacuum chamber, is applied parallel to the film surface. The coercive field is 20 Oe. During deposition of the Co film and the measurement of the hysteresis loop the substrate was held at room temperature. According to Refs. 8, 16, and 17 deposition at room temperature gives rise to layer-by-layer growth. In agreement with Ref. 8 we did not observe any change in the magnetic properties up to -150 °C. The experiment was performed in a vacuum which never exceeded 5×10^{-10} mbar.

(3) The in-plane square hysteresis loop for films ranging from 1 to 10 ML and the absence of remanence perpendicular to the film plane observed in Ref. 8 demonstrate that the spins lie exactly in the film plane; i.e., no evidence of the transition[5] from perpendicular to in-plane magnetization upon increasing the thickness is observed.

Figure 1 shows that the conventional concepts of ferromagnetism, like hysteresis loop, coercive field, and domains can be straightforwardly extended to systems as thin as 1 ML. The size and shape of these domains remain a topic for future research.

The findings of this paper identify Co/Cu(100) as a truly epitaxial ferromagnetic monolayer. In the course of this work a similar system, fulfilling the criterion as well, has been discovered[21]: Fe/Au(100). Provided the substrate is held at room temperature during deposition, distinct breaks can be detected in the Auger signal of the substrate versus deposition time,[22] signaling the occurrence of layer-by-layer growth. In our laboratory the magnetization of the system was measured with the standard technique of spin-polarized LEED.[23] Because of

the exchange part of the Coulomb potential, low-energy (typically 10–50 eV) incident electrons with spin parallel to the sample magnetization and those with spin antiparallel are reflected with different intensities, $R_\uparrow$ and $R_\downarrow$, respectively. Therefore, *provided the film has a magnetization different from zero*, a spin asymmetry $A_m=(R_\uparrow-R_\downarrow)/(R_\uparrow+R_\downarrow)$ results. Because of the use of low-energy electrons, measurements have to be performed in zero applied magnetic field; i.e., A_m *measures the remanent magnetization*. As a consequence, a full hysteresis loop is not yet available. While the mechanism of magnetization reversal is not known, for 1 ML of Fe on Au(100) at 0°C we measure (i) values of A_m as large as $10\%\pm0.3\%$ (depending on the angle of incidence and the energy of the electrons)[24]; i.e., the film has a finite remanence M_R. Moreover, (ii) M_R could be switched to $-M_R$ by the application of a coercive field as low as 2 Oe. (i) and (ii) establish the ferromagnetism of a monolayer of Fe on Au(100) according to the stringent criteria used in this paper.

Evidently, provided the interface is sharp and the amount of defects in the film is low enough, the physical realization of ferromagnetic monolayers of 3*d* transition metals is within the reach of experimental physics.

One of us (T.B.) thanks the Institut für Festkörperforschung der Kernforschungsanlage for the kind hospitality.

[1]N. D. Mermin and H. Wagner, Phys. Rev. Lett. 17, 1133 (1966); see also D. C. Mattis, *The Theory of Magnetism II* (Springer-Verlag, Berlin, 1985), pp. 69–88.

[2]C. L. Fu, A. J. Freeman, and T. Oguchi, Phys. Rev. Lett. 54, 2700 (1985).

[3]R. Richter, J. G. Gay, and J. R. Smith, Phys. Rev. Lett. 54, 2704 (1985).

[4]H. Hasegawa, Surf. Sci. 182, 591 (1987).

[5]J. G. Gay and R. Richter, J. Appl. Phys. 61, 3362 (1987).

[6]M. Przybylski and U. Gradmann, Phys. Rev. Lett. 59, 1152 (1987).

[7]D. Pescia, M. Stampanoni, G. L. Bona, A. Vaterlaus, R. F. Willis, and F. Meier, Phys. Rev. Lett. 58, 2126 (1987).

[8]D. Pescia, G. Zampieri, M. Stampanoni, G. L. Bona, R. F. Willis, and F. Meier, Phys. Rev. Lett. 58, 933 (1987).

[9]S. D. Bader and E. R. Moog, J. Appl. Phys. 61, 3729 (1987).

[10]M. Stampanoni, A. Vaterlaus, M. Aeschlimann, and F. Meier, Phys. Rev. Lett. 59, 2483 (1987).

[11]B. T. Jonker, K. H. Walker, E. Kisker, G. A. Prinz, and C. Carbone, Phys. Rev. Lett. 57, 142 (1986).

[12]B. Heinrich, K. B. Urquhart, A. S. Arrot, J. F. Cochran, K. Myrtle, and S. T. Purcell, Phys. Rev. Lett. 59, 1756 (1987).

[13]M. C. Koos, B. T. Jonker, F. A. Volkening, J. J. Krebs, and G. A. Krebs, Phys. Rev. Lett. 59, 2463 (1987).

[14]C. Liu, E. R. Moog, and S. D. Bader, Phys. Rev. Lett. 60, 2422 (1988).

[15]W. A. A. Macedo and W. Keune, Phys. Rev. Lett. 61, 475 (1988).

[16]A. Clarke, G. Jennings, R. F. Willis, P. J. Rous, and J. B. Pendry, Surf. Sci. 187, 327 (1987).

[17]L. Gonzales, R. Miranda, M. Slameron, J. A. Verges, and F. Yndurain, Phys. Rev. B 24, 3248 (1981).

[18]J. A. C. Bland, D. Pescia, and R. F. Willis, Phys. Rev. Lett. 58, 1244 (1987).

[19]J. V. Jose, L. P. Kadanoff, S. Kirkpatrick, and D. R. Nelson, Phys. Rev. B 16, 1217 (1977).

[20]W. J. Tabor, in *Laser Handbook*, edited by F. T. Arecchi and E. O. Schulz-Du Bois (North-Holland, Amsterdam, 1972), p. 1023.

[21]The possibility of Fe/Au(100) being a truly epitaxial ferromagnetic monolayer has been suggested simultaneously by W. Dürr, R. Germar, and D. Pescia (Jülich), private communication, and by M. Taborelli, O. Paul, and M. Landolt (Eidgenössische Technische Hochschule Zürich), private communication.

[22]As reported by Bader and Moog, Ref. 9, the Auger signal of the substrate—for the deposition conditions given in Ref. 9 (substrate temperature 230°C)—does not decrease exponentially with deposition time, signaling the break down of layer-by-layer growth. We find that when the substrate is held at room temperature during deposition and not at 230°C as in Ref. 9, layer-by-layer growth occurs; see R. Germar, W. Dürr, J. W. Krewer, D. Pescia, and W. Gudat, to be published.

[23]S. F. Alvarado, R. Feder, H. Hopster, F. Ciccacci, and H. Pleyer, Z. Phys. B 49, 123 (1982).

[24]Notice that, for the Kerr intensity I in Fig. 1, $[I(H=60\ \text{Oe})-I(H=-60\ \text{Oe})]/[I(H=60\ \text{Oe})+I(H=-60\ \text{Oe})]$ is about 2 orders of magnitude smaller than A_m, because of the large probing depth of an optic experiment compared to the short probing depth (2–3 ML) of low-energy electron diffraction.

The question is: what is the true origin of the observed long range order?

The answer lies in the unusual responce of a 2d-system to minute deviations from the pure isotropic exchange interaction. As an example of such response, consider an in plane uniaxial anisotropy $-\frac{1}{2}K\cdot\sum_{\vec{x}}\left(S_x^2(\vec{x})-S_y^2(\vec{x})\right)$. This term removes the degeneracy of the ground state with minimum energy corresponding to the total spin along the x-axis. Introducing as usual the vector $\vec{S}=S\cdot(\cos\omega(\vec{x}),\sin\omega(\vec{x}))$ the extra term becomes $-\frac{1}{2}S^2K\sum_{\vec{x}}\cos 2\omega(\vec{x})$. Within the spin wave approximation $-\frac{1}{2}S^2K\sum_{\vec{x}}\cos 2\omega(\vec{x})\sim$

$$-\tfrac{1}{2}K\cdot S^2\cdot\frac{4}{2}\omega^2(\vec{x})=+K\cdot S^2\cdot\omega^2(\vec{x})\longrightarrow K\frac{S^2}{a^2}\int\omega^2(x)\cdot d^2x.$$

The Hamilton operator of the system in k-representation is therefore $\frac{1}{2}J\sum_k k^2\cdot|\omega_k|^2+\frac{KS^2}{a^2}\cdot\sum_k|\omega_k|^2$.

which we use to obtain

$$\langle|\omega_k|^2\rangle=\frac{\int d\omega_k\,\omega_k^2\cdot e^{-\left[\frac{1}{2}Jk^2+\frac{KS^2}{a^2}\right]/T\cdot\omega_k^2}}{\int d\omega_k\,e^{-\left[\frac{1}{2}Jk^2+KS^2/a^2\right]/T}}=$$

$$=\frac{T}{Jk^2+2KS^2/a^2}$$

The magnetization at finite temperatures is

again $S \cdot e^{-\frac{1}{2}\langle \omega^2(x)\rangle}$ so that what is left to do is to calculate $\langle \omega^2(x)\rangle$.

$$\langle \omega^2(x)\rangle = \frac{1\cdot 2\pi}{(2\pi)^2}\int d\vec{k}\cdot k \cdot \frac{T}{\tilde{J}k^2 + 2Ks^2/a^2} = \frac{1}{2\pi}\frac{T}{2\tilde{J}}\int \frac{2\cdot \tilde{J}k\cdot dk}{\tilde{J}k^2 + 2Ks^2/a^2} =$$

$\tilde{J}k^2 = x \qquad \tilde{J}(2\pi/a)^2$

$$= \frac{T}{4\pi\tilde{J}}\int_{\tilde{J}(\frac{2\pi}{L})^2}^{\tilde{J}4\pi/a^2} \frac{dx}{x + 2Ks^2/a^2} = \frac{T}{4\pi\tilde{J}}\ln\left(x + 2Ks^2/a^2\right)\Big|_{\tilde{J}4\pi^2/L^2}^{\tilde{J}4\pi/a^2} =$$

$$\overset{L\to\infty}{=} \Delta\cdot \ln\frac{\tilde{J}4\pi/a^2 + 2Ks^2/a^2}{2Ks^2/a^2} = \Delta\cdot\ln\left(1 + \frac{2\pi\tilde{J}}{Ks^2}\right) \cong$$

$$\Delta\cdot\ln\left(\frac{2\pi\tilde{J}}{Ks^2}\right).$$

$$\underline{\underline{S\cdot e^{-\frac{1}{2}\langle \omega^2(x)\rangle}}} = S\cdot e^{-\frac{1}{2}\Delta\cdot\ln(2\pi\tilde{J}/Ks^2)} = \underline{\underline{S\cdot\left(\frac{Ks^2}{2\pi\tilde{J}}\right)^{\Delta/2}}}.$$

This result shows a quite remarkable property: an infinitesimally small - but finite - anisotropy is enough to install the full magnetization at finite temperatures. This is because, no matter how small $K/\tilde{J}$ is, the exponent Δ is so small (at low temperatures), that $(K/\tilde{J})^{\Delta}$ is of the order of 1-S. The interested student might find it interesting to repeat the same calculation for the case where the disturbance from pure exchange is provided by the

dipole-dipole interaction: the Hamilton operator is then $\frac{\tilde{J}}{2}\int(\vec{\nabla}\omega)^2 d^2x + \frac{1}{2}(g\mu_B S)^2\frac{1}{a^4}\iint d^2\vec{x}\,d^2\vec{x}'\,\frac{\vec{m}(\vec{x})\cdot\vec{m}(\vec{x}')}{|\vec{x}-\vec{x}'|}$.

The result is very similar to the previous one:

$$S\cdot e^{-\frac{T}{\tilde{J}}\langle\omega^2(x)\rangle} \sim S\cdot\left(\frac{2\pi(g\mu_B S)^2}{\tilde{J}a^3}\right)^{\frac{\Delta}{1}}$$: again, an interaction as weak as the dipole interaction is enough to switch a long range order of the order of S at finite temperatures!! The existence of long range order at finite temperature is no longer mysterious, even for truly 2d-systems, but is a natural consequence of the unusual response of a 2d-system to minute interactions. As a matter of fact, both anisotropies and spin waves - the key ingredients in this picture of 2d-magnetism, have been found experimentally in a truly epitaxial system Co/Cu (100).

spontaneous magnetization (four-fold magnetic anisotropy). Accordingly, the spectrum of the spin waves should have a gap, whose energy is of the order of 400 $Oe/\mu = 10^{-1}$ K. To access the spin waves in this system we have used inelastic light scattering. In this technique[20] a laser (typically a 300 mW Argon-laser with 514.5 nm wavelength) provides the incident beam. The intensity of the photons scattered at a certain angle (different from the reflection angle!) is then measured as a function of the energy shift of the scattered photons, see Fig. 17. Apart from being elastically scattered in all directions (so-called Rayleigh scattering) — as a consequence of, e.g., deviations from perfect flatness — photons in general may lose or gain energy by exciting or absorbing phonons and magnons. Once the phonon contribution has been filtered out from the spectra (using, for instance, crossed linear polarizers to analyse the incident and scattered beam[20]), the 1 ML Co/Cu(100) showed a well-defined peak on the gain side of the spectrum, caused by the absorption of spin waves, see Fig. 17. The energy of this long wavelength

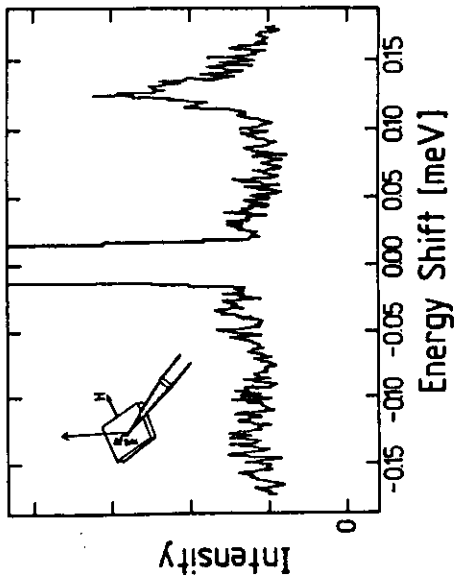

Fig. 17. Intensity of the scattered light versus energy shift, at room temperature and in an applied magnetic field of 3 kOe. The sample consisted of a 1 ML Co sandwiched between Cu. The coating was around 30 Å, the substrate was a (100)-surface. The inset shows the geometry at which the spectrum was taken: the scattered light is measured in the back scattering geometry (the arrow indicates the direction of the specularly reflected light), while the magnetic field is applied perpendicular to the direction of incidence. In this geometry, magnons propagating with a wavelength of 363 nm perpendicular to the magnetic field direction are detected.

our two-dimensional model systems. The next logical step is the search for evidence of spin waves and magnetic anisotropies in our systems.

For the 1 ML Co/Cu(100) we measured hysteresis curves as a function of the angle ψ between the applied magnetic field and an in-plane crystallographic axis, see Fig. 16. Along the easy axis ($\psi = 45°$) saturation occurs at th coercive field (a few Oersteds), while at $\psi = 90°$ and 0° saturation occurs at aro ind 400 Oe. The system is indeed magnetically anisotropic, as expected fro n our observed

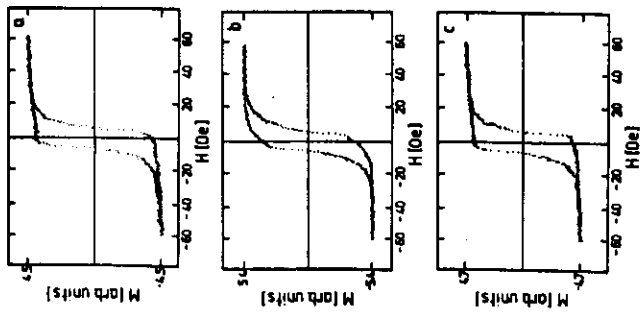

Fig. 16. Hysteresis loops for the system Cu/1 ML Co/Cu(001) with applied magnetic field along different in-plane crystallographic directions. a) H along [100]; b) H along [110], which is 45° away from the [100] and; c) H along [010], which is 90° away from the [100]. The four-fold symmetry is evident from a) and c) being identical. In b) saturation is achieved at about the coercive field, while in a) and c) saturation is achieved at about 400 Oe.

From the spin wave approximation, one obtains the curious result that $\langle s \cdot e^{iw(x)} \rangle \xrightarrow[T\to\infty]{} 0$, i.e there is no phase transition. This anomaly is not confirmed by experimental observations, which show the occurrence, in epitaxial films, of an ordinary second order phase transition at a well defined Curie temperature.

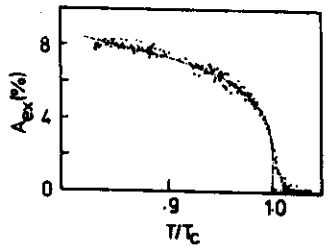

Fig. 21. Temperature dependence of the spin asymmetry A_{ex} of the 60-LEED beam from 1 ML Fe on Au(100). The angle of incidence of the electron beam was 22°, its energy 17 eV. The continuous curve through the data points is the power law function $M = \text{const.}\ (1 - T/T_c)^{\beta}$, where the const and β were determined by minimizing the square of the sum of the errors between the data points and the fitting function. T_c was chosen to maximize the range of temperatures over which a power law holds true.

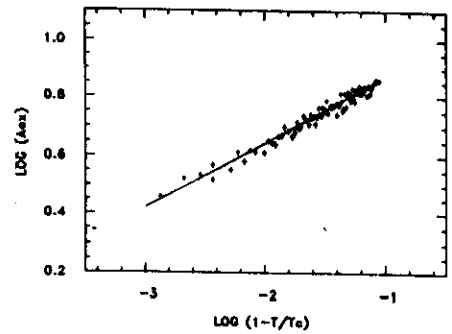

Fig. 22. Log-log plot of the data of Fig. 21, between $0.9 < T/T_c < 1.0$. On this scale a power law singularity should be represented by a straight line, as indeed is the case. The slope of the straight line is the critical exponent β, which in this case is 0.22.

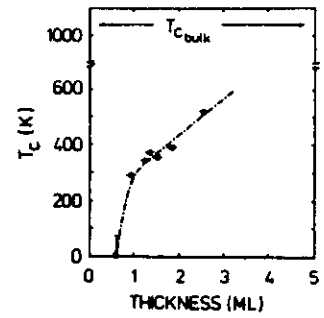

Fig. 20. Thickness dependence of the Curie temperature T_c as determined by measuring spontaneous magnetization as a function of T.

Measurements performed with the method of Spin Polarized Low Energy Electron Diffraction.

The origin of the phase transition must lie in the anharmonic terms neglected in favour of the $(w(\vec{x}+\vec{a})-w(\vec{x}))^2$- term! We show the existence of a well-defined temperature at which M disappear by means of a method developed by Pokrovskii et al. This method consists of approximating the exact Hamiltonian $-J S^2 \sum_{\vec{x},\vec{a}} \cos(w(\vec{x}+\vec{a})-w(\vec{x}))$ not by $\frac{J}{2}\int(\nabla w)^2 d^2x$ but by $\frac{J}{2}\cdot\rho_s\cdot\int(\nabla w)^2 d^2x$, where ρ_s is a parameter to be determined and should incorporate the effect of the anharmonic terms. The method of determining ρ_s is based on an inequality by Bogoliubov. Let us write the exact Hamiltonian as

$$H = \underbrace{\tfrac{1}{2}J\rho_s\int(\nabla w)^2}_{H_0} + \underbrace{\left(-J\cdot S^2\sum_{\vec{x},\vec{a}}\cos(w(\vec{x}+\vec{a})-w(\vec{x})) - \tfrac{1}{2}J\cdot\rho_s\int(\nabla w)^2 d^2x\right)}_{H_1}.$$

In general, $F(H) \leq F(H_0) + \langle H_1\rangle_0$, where $\langle H_1\rangle_0$ means that the statistical weight is calculated with the Hamiltonian H_0. ρ_s is then chosen so that $\frac{\partial[F(H_0)+\langle H_1\rangle_0]}{\partial\rho_s} = 0$, i.e. the right hand side of the inequality has a minimum. Provided

$H_1 \ll H_0$, this minimum value will approach closely the true $F(H)$, and the choice of ρ_s will be physically relevant. We want now to carry out this scheme explicitely.

$$F(H_0) + \langle H_1\rangle_0 = \langle H\rangle_0 - T\cdot S_0$$

$$H = \langle -J\cdot S^2\sum_{\vec{x},\vec{a}}\cos(w(\vec{x}+\vec{a})-w(\vec{x}))\rangle_0 =$$

$$= -J\cdot S^2\sum_{\vec{x},\vec{a}}\langle\cos(\vec{w}(\vec{x}+\vec{a})-w(\vec{x}))\rangle_0 =$$

$$= -J\cdot S^2\cdot z\cdot N\cdot e^{-\frac{1}{2}}\langle(w(\vec{x}+\vec{a})-w(\vec{x}))^2\rangle_0$$

N: total number of atoms. z: nearest neighbours.

Because $\langle(w(\vec{x}+\vec{a})-w(\vec{x}))^2\rangle = 2\left[\langle w^2(\vec{x})\rangle - \langle\vec{w}(\vec{x})\cdot w(\vec{x}+\vec{a})\rangle\right]$

we obtain:

$$\langle(w(\vec{x}+\vec{a})-w(\vec{x}))^2\rangle = \frac{2}{(2\pi)^2}\cdot\int d^2k\,\langle w_k^2\rangle\left(1-e^{i\vec{k}\cdot\vec{a}}\right)$$

where we have used the continuum limes. $\int d\Theta$ leads to $\langle\dots^2\rangle = \frac{1}{\beta}\frac{2\cdot I}{2\pi\cdot J}\int_0 k\cdot dk\cdot\frac{1}{k^2}\left(1-J_0(ka)\right)$,

where J_0 is a Bessel function. The integration range for k is $0 \sim \frac{1}{a}$, where the exact value of the upper limit cutoff remains at this stage a disposable parameter, later determined by the

physically plausible condition $\rho_s(T=0)=1$.
In summary:

$$\langle H\rangle_0 = -2\cdot\tilde{J}\cdot N\cdot e^{-\frac{T}{\pi c\tilde{J}\cdot\rho_s}}.$$

$$S_0 = -\frac{\partial F(H_0)}{\partial T} = \frac{\partial}{\partial T} T\ln Z_0 = \ln Z_0 + T\cdot\frac{\partial}{\partial T}\ln Z_0$$

$$Z_0 = \int dw_{k_1}\dots dw_{k_m}\, e^{-\frac{1}{2}\tilde{J}\cdot\rho_s\cdot\frac{1}{T}\cdot\sum_i k_i^2|w_{k_i}|^2} =$$

$$= \prod_{k_i}\int dw_{k_i}\cdot e^{-\frac{\tilde{J}}{2}\rho_s\cdot\frac{1}{T}\cdot k_i^2\cdot|w_{k_i}|^2} = \prod_{k_i}\frac{\sqrt{\pi}\cdot\sqrt{T}\cdot\sqrt{2}}{2\cdot\sqrt{\tilde{J}\cdot\rho_s}\cdot k_i}$$

Up to a constant, $S_0 = \frac{1}{2}\cdot\sum_k \ln\frac{\pi\cdot T}{2\cdot\tilde{J}\cdot\rho_s\cdot k^2}$.

$$\Rightarrow \frac{\partial H_{S_0}}{\partial\rho_s} - \frac{\partial T\cdot S_0}{\partial\rho_s} = -\frac{2\cdot\tilde{J}\cdot N\cdot T}{\pi c\tilde{J}}\cdot\frac{e^{-\frac{T}{\pi c\tilde{J}\rho_s}}}{\rho_s^2} +$$

$$+ T\cdot\frac{1}{\rho_s}\cdot\frac{N\cdot a^2}{(2\pi)^2}\overbrace{\int d^2k}^{c'^{-1}} = 0 \Rightarrow \rho_s = \frac{c'}{c}\cdot\frac{2}{\pi}\cdot e^{-\frac{T}{c\cdot\pi\cdot\tilde{J}\cdot\rho_s}}$$

where the integration limit for k is to be chosen so that $c'/c\cdot\frac{2}{\pi}=1$. The following equation for ρ_s is $\underline{\rho_s = e^{-\theta/\rho_s}}$, where

$\theta = T/c\tilde{J}$ is the temperature of the system measured in units of $c\cdot\tilde{J}$. At $\theta=0$, $\rho_s=1$, has required. At finite θ, $\rho_s=0$ is always a

solution. Our suspicion that, at low temperatures, the spin wave approximation should be correct leads us to search for another solution, with $\rho_s\neq 0$ at sufficiently low temperatures. To find this solution we introduce the variable $y=\theta/\rho_s$ and solve the equation $e^y = y/\theta$ graphically.

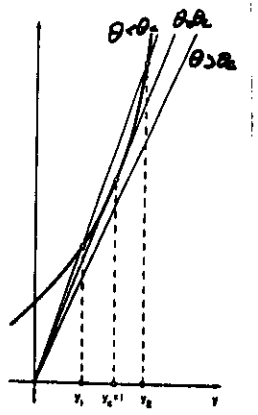

At a given slope θ_c, the straight line y/θ_c touches e^y. The equation has a non-trivial solution $y_c=1$, $\theta_c=\rho_{sc}=e^{-1}$. For "temperatures" $\theta>\theta_c$ the only solution is indeed $\rho_s=0$, while for $\theta<\theta_c$ there is always a non trivial solution $\rho_s\neq 0$, see the following figure.

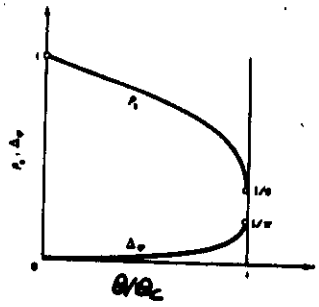

The main result of the anharmonic terms is to "renormalize" the exchange constant $\tilde{J}$ according to $\tilde{J}\cdot\rho_s$. This "renormalization" introduces a temperature in the system, at which the phase encountered within the spin wave approximation, collapses. In particular, for the long range order parameter $\sim(K)^{\Delta/2}$ or $((g\mu_B)^2)^{\Delta}$,

one has to take into account that $\Delta = \frac{T}{4\pi \tilde{J}}$ becomes $\Delta = \frac{T}{4\pi J \rho_s}$. Above θ_c, $\Delta = \infty$ and there is no long range order. Below θ_c, a finite magnetization exists.

This important result, which is in line with the experimental observation of a phase transition, has been obtained by a variational method. More accurate calculations, which take into account the formation of vortices, show that $\Delta_c = 1/8$, i.e. the variational method overestimate slighly the value of θ_c (or, alternatively, underestimate the value of ρ_s at T_c). The physical picture of 2d-magnetism remains, however, unaffected by such quantitative details: minute deviations from the pure isotropic exchange interactions violate the Mermin-Wagner theorem and lead to a finite long range order at finite temperatures. There exists a temperature at which the system looses this long range order: this temperature is well defined, the value of Δ_c being exactly $1/8$ (universal value).

It remains to be explained, how the system crosses over to conventional power laws in the

vicinity of T_c, as observed experimentally. (the crude variational approach does not explain this). The physics of 2d-system within the critical region $\frac{T-T_c}{T_c} \ll 1$ is too complicated to be death with in this lectures. Actually, some important facts are, surprisingly, still missing: nobody knows, for instance, what is the role of the dipole-dipole interaction in the critical range. We summarize, for your benefit, some well established facts for two- and four fold in plane anisotropies (which is experimentally relevant, being the case of Fe/W(110) and Co/Cu(100), respectively).

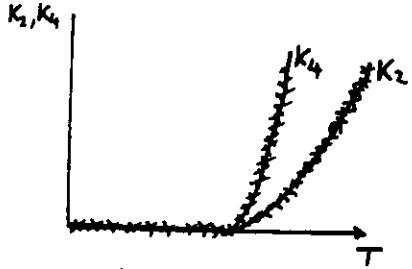

In the K-T-plane, there are lines of second order phase transitions. At $K_2 = K_4 = 0$ the phase is characterized by a finite ρ_s but no long range order. At finite K's - long range order occurs. Upon crossing the critical lines, the various thermodynamical quantities follow ordinary power laws, with Ising-like critical exponents across K_2 (Ising model: $H_{ising} = -J \sum_i S_i^{(z)} S_j^{(z)}$). In particular β in

$M \sim (1 - T/T_c)^{\beta}$ is expected to be the famous

1/8-value, derived first by C.N. Yang on the basis of the Onsager solution. Across K_4, only for $K_4 \gg 0$ Ising-like critical exponents are realized. Elsewhere, the critical exponents are <u>non-universal</u>, i.e. they depend on the strength of K_4.

Jülich, 10.5.1990

D. Pesa